LAWRENCE
LIVERMORE
NATIONAL
LABORATORY

LLNL-JRNL-826634

Wavefront shaping with Hadamard basis for highly scattering soil imaging

D. Wang, L. A. Poyneer, D. Chen, S. M. Ammons, K. D. Morrison, J. Lee, S. S. Ly, T. A. Laurence, P. K. Weber

September 13, 2021

Applied Optics

Disclaimer

Wavefront shaping with Hadamard basis for scattering soil imaging

DONGPING WANG,[1,*] LISA A. POYNEER,[1] DIANA CHEN,[2] S. MARK AMMONS,[3] KEITH D. MORRISON,[4] JANGHYUK LEE,[5] SONNY S. LY,[5] TED A. LAURENCE,[5] AND PETER K. WEBER[4]

[1]*Computational Engineering Division, Engineering, Lawrence Livermore National Laboratory, Livermore, California 94550, USA*
[2]*Laser Systems Engineering and Operations, Engineering, Lawrence Livermore National Laboratory, Livermore, California 94550, USA*
[3]*Physics Division, Physical & Life Sciences, Lawrence Livermore National Laboratory, Livermore, California 94550, USA*
[4]*Nuclear and Chemical Sciences Division, Physical & Life Sciences, Lawrence Livermore National Laboratory, Livermore, California 94550, USA*
[5]*Materials Science Division, Physical & Life Sciences, Lawrence Livermore National Laboratory, Livermore, California 94550, USA*
**Corresponding author: wang119@llnl.gov*

Abstract: Soil is a scattering media that inhibits imaging of plant-microbial-mineral interactions that are essential to plant health and soil carbon sequestration. However, optical imaging in the complex media of soil has been stymied by the seemingly intractable problems of scattering and contrast. Here we develop a wavefront shaping method based on adaptive stochastic parallel gradient descent optimization with Hadamard basis to focus light through soil mineral samples. Our approach allows a sparse representation of the wavefront with reduced dimensionality for the optimization. We further divide the used Hadamard basis set into subsets and optimize a certain subset at once. Simulation and experimental optimization results demonstrate our method has a ~7 times higher convergence rate and overall better performance compared to that with optimizing all pixels at once. The proposed method can benefit other high-dimensional optimization problems in adaptive optics and wavefront shaping.

1. Introduction

Plant-microbiome interactions are a critical determinant of plant health and organic matter turnover in soil [1-4]. Advancing our ability to visualize these interactions is crucial to studies of C cycling, sustainable food and biofuel production. However, optical imaging in the complex media of soil has previously been stymied by the seemingly intractable problems of scattering and contrast in soil. In the last decade, it has become increasingly clear that scattering need not be a fundamental limitation for imaging. The scattering process is complex yet deterministic and the light focused through the scattering media can be controlled [5].

Wavefront shaping has been developed to focus light through [6] or inside scattering media [7]. Representing different ends of the scattering spectrum, conventional adaptive optics (AO) techniques work in the regime of aberration correction by expanding the wavefront in Zernike modes, whereas wavefront shaping techniques are conceived for the regime of scattering where the wavefront is heavily distorted [5]. Therefore, AO normally employs a wavefront sensor to measure aberrations, whereas wavefront shaping often relies on feedback signals to improve the image quality metric. By shaping the incident wavefront, light can be manipulated and focused deep inside strongly scattering objects. Iterative feedback-based optimization algorithms for wavefront shaping to focus light in the presence of scattering have been demonstrated, such as genetic algorithm [8], random partitioning algorithm [9], hill climbing

[10], random search methods [10] and stochastic parallel gradient descent (SPGD) [11]. Among these, SPGD is a parallel method yielding faster convergence [11] than the other methods by perturbing all the degrees of freedom simultaneously along the stochastic gradient direction. However, for complex high-dimensional optimization problem, SPGD leads to low convergence rate and high probability of falling into local optima [12].

An advanced version of SPGD, called adaptive stochastic parallel gradient descent (ASPGD) algorithm has been proposed for efficient fiber coupling [13] and laser beam cleanup [14]. ASPGD is inspired by the algorithm Adam [15], which integrates the momentum and the adaptive gain coefficient estimation to SPGD in order to improve the convergence rate and reduce the probability of falling into the local optima suffered from SPGD [13]. However, for the wavefront shaping application in soil imaging, the number of control variables can reach hundreds to a few thousands, which means ASPGD needs to search in hundreds to thousands control variable space. With the massive expansion of dimension, even ASPGD results in laggard optimization progress.

One solution to reduce the overwhelming dimensionality for ASPGD optimization is to adopt an appropriate control basis, which can facilitate a sparse representation of the wavefront. This sparse representation only has large coefficients in the region of dominant modes. The rest of the coefficients are sufficiently small and may be set exactly equal to zero with negligible loss of quality [16]. Therefore, a well-chosen basis requires fewer modes to characterize the wavefront, which in turn reduces the dimensionality of the optimization. The Hadamard basis is a complete orthogonal basis set [17-18] which enables a sparse representation of the soil wavefront, allowing us to acquire the spatial information of the soil wavefront structure and characterize it with less coefficients. In previous works, Hadamard basis has been used in transmission matrix measurement [19-21], single-pixel detection and image reconstruction [22], and sequential optimization [23] in scattering imaging.

In this paper, we present a wavefront shaping method based on parallel ASPGD with modified Hadamard basis as the control basis for focusing through soil mineral samples. Compared with other commonly used basis, such as pixel basis, Hadamard basis holds the ability of reducing the dimensionality of the optimization; Compared with the Zernike polynomial basis [24] that is widely used in representing optical aberrations, the Hadamard basis is a universal complete orthogonal basis, which can represent any arbitrary wavefront. ASPGD with Hadamard basis allows a sparse representation of the wavefront with reduced dimensionality in the control space. We further divide the selected Hadamard basis set into different subsets: a subset of modes is optimized then frozen, while another subset is then optimized, which in turn accelerates the optimization process.

2. Methods

2.1 ASPGD algorithm working principles

ASPGD is an iterative stochastic gradient descent optimization method. The gradient estimation g^k of the system performance metric J is calculated by simultaneously applying random perturbations $\pm\delta u^k = \pm\{\delta u_1^k, \delta u_2^k, \dots, \delta u_n^k\}$ to all the control variables $u^k = \{u_1^k, u_2^k, \dots, u_n^k\}$ and measuring the variation of system performance metric δJ caused by the perturbations. n is the number of control variables, k indicates the current iteration, δu^k have identical amplitudes which satisfy Bernoulli probability distribution. To increase the convergence rate, the 1st momentum m^k, which is exponential moving average of the past gradients, is introduced. To adaptively adjust the gain rate for different variables, the 2nd momentum v^k is introduced which sums up the weighted square results of the past gradients. β_1 and β_2 are exponential decay rate hyper-parameters controlling the decay rates of the 1st and 2nd momentum in the previous steps. To correct the moment estimates that are biased towards zero, especially during the initial timesteps, bias-corrected 1st and 2nd moment estimates, $\widehat{m^k}$ and $\widehat{v^k}$ are used [15]. In the optimization process, the control variables are updated as follows:

$$u^{k+1} = u^k + \alpha \cdot \widehat{m^k} / \sqrt{\widehat{v^k} + \varepsilon} \quad (1)$$

where α is the update step-size and ε is a small positive number to avoid division by zero.

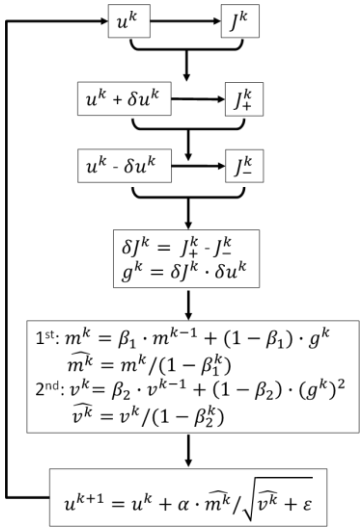

Fig. 1. Flowchart of ASPGD working principles.

2.2 Orthogonalization of Hadamard basis over a circular pupil

There are different representations of control variable space u^k, such as individual or binned pixel basis, Fourier basis and Zernike polynomial basis. However, the pixel basis is an overcomplete set [18] with high dimensionality and leads to slow convergence speed. The Fourier basis can cause quantization errors when using a phase-only spatial light modulator (SLM) to generate Fourier basis patterns [18]. The Zernike polynomial basis [24] usually represents lower-order aberration modes that are not suitable for imaging applications in the presence of scattering [5]. On the other hand, the Hadamard basis is a universal complete orthogonal basis, which perfectly fits with the use of SLM [19], can represent any arbitrary wavefront and holds the ability of reducing the dimensionality of the representation.

The Hadamard basis is derived from the Hadamard matrix: a square matrix with elements ±1 whose rows (or columns) are orthogonal to each other [17]. Each Hadamard basis pattern is formed by reshaping a row (or a column) of the Hadamard matrix into a two-dimensional square array. To accommodate the fact that the Hadamard basis pattern will represent the wavefront with a wrapped phase range from 0 to 2π, we replace the elements -1 with 0. Figure 2 shows an exemplary Hadamard basis set with order of 4. Figure 2(a) shows the original Hadamard basis set. First, we re-order the original Hadamard basis set such that the modes representing lower frequencies will have a lower index when we reshape the 4-by-4 Hadamard basis array into a 16-by-1 vector for the sake of programming convenience, as shown in Fig. 2(b). Next, considering our optical system has a circular pupil shape, we multiply the rectangular Hadamard basis pattern with our circular pupil mask, and then conducted Gram-Schmidt orthogonalization [25] to the new circular Hadamard basis set and finally obtain an orthogonalized Hadamard basis set over the circular pupil, as shown in Fig. 2(c). By orthogonalizing the Hadamard basis over the circular shape, any subset of Hadamard basis can approximate a wavefront pattern with a circular pupil. Without doing so, the complete set of square Hadamard basis is needed to represent a wavefront pattern with a circular pupil.

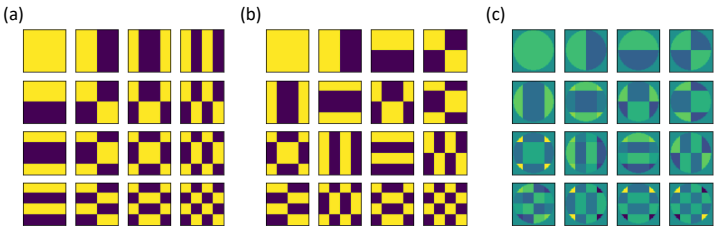

Fig. 2. Hadamard basis. (a). Original Hadamard basis set. (b). Re-ordered Hadamard basis set. (c). Re-ordered orthogonalized Hadamard basis set over a circular pupil.

2.3 Dimensionality reduction with Hadamard basis

Figure 3(a) shows a simulated soil phase map based on the power spectral density (PSD) model derived from scatterometer measurements (ScatterScope4, The Scatter Works, Inc.) on a synthetic smectite sample [26]. Smectite is a common soil mineral that allows us to have a standardized sample. Firstly, the scatterometer measurements are converted to radial average profile of the point spread function (PSF). Secondly, the PSF radial average profile is fit to the PSD model to obtain the soil wavefront characteristics and coefficients which model the aberration and distortion distribution caused by the sample. A random soil phase profile is generated from the PSD using standard noise filtering methods. The modified Hadamard basis set is used to represent the soil phase map. The dimension of the phase map is 848 × 848, which is consistent with the dimension of the pupil on the SLM in the experimental setup (see section 3.2). The Hadamard basis set we are using to decompose the soil phase is of order of 32 and the total number of modes is 812 after orthogonalization over the circular pupil. We combine a block of 26 × 26 pixels to represent one binned pixel. Figure 3(b) plots the Hadamard coefficient for each mode in the decomposition of the soil phase. It can be observed that lower order Hadamard basis modes (corresponding to lower spatial frequencies) have larger coefficients, indicating that they have more impact in representing the soil phase; higher order Hadamard basis modes (corresponding to higher spatial frequencies) have smaller coefficients, indicating less impact in representing the soil phase.

To verify the observation and quantify the impact, Fig. 3(d) shows the soil phase approximation with different truncated sets of Hadamard basis and the corresponding partially corrected PSF, which indicates the ability of a system to correct the soil phase using only these modes. The PSF is modeled on a 3647 × 3647 grid size with 848 × 848 pixels across the pupil. It is computed with Fraunhofer propagation of the difference between the full soil phase and the soil phase approximation with a truncated set of Hadamard basis. To have a better visualization effect, Fig. 3(c) plots the Strehl ratio improvement of the partially corrected PSF with the number of Hadamard basis mode used to approximate the soil phase. It shows that PSF correction performance improves with the increasing number of Hadamard basis mode used to approximate the soil phase; The improvement is rapid in the low order Hadamard basis range, and there is only a marginal improvement in the high order Hadamard basis range even with a large number of modes, which is consistent with the observation of Hadamard coefficient distribution in Fig. 3(b). This is expected given the power law structure of the soil phase map, which indicates that most of the wavefront power is in the lower-frequency Hadamard modes, so correction those first has the largest impact on the correction, whereas the higher-frequency Hadamard modes have less impact. This means a truncated set of Hadamard basis can approximate the soil phase with a good balance between correction performance and number of modes used. This reduces the dimensionality of the soil phase representation and consequently reduces the optimization dimensionality of wavefront shaping in soil imaging. This will lead to a faster convergence rate.

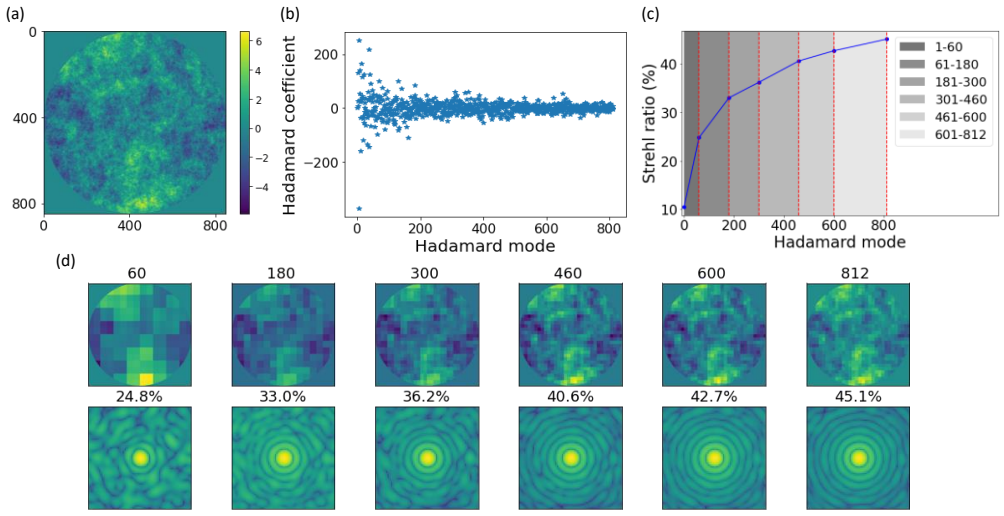

Fig. 3. Soil phase decomposition and approximation with Hadamard basis. (a). Simulated soil phase. (b). Soil phase decomposition with Hadamard basis. (c). PSF correction performance plot with truncated sets of Hadamard basis. (d). Visualization of soil phase approximation with truncated sets of Hadamard basis (upper row) and the corresponding partially corrected PSF (bottom row).

3. Results

3.1 Simulation results

The system modeling and ASPGD algorithm are developed in Python. PSFs are estimated with Fraunhofer propagation via Fast Fourier Transform. For the implementation of ASPGD algorithm (in both simulation and experiment), the default hyper-parameter setting, e.g., $\beta_1 = 0.9$, $\beta_2 = 0.999$, and $\varepsilon = 1e^{-8}$ are kept constant, while learning rate α and the amplitude of random perturbations $|\delta u^k|$ are varied in order to obtain the optimal optimization performance for each scenario (see supplementary materials for details). Besides, we reduce the learning rate in an exponential decay fashion as the optimization progresses, e.g., $\alpha_k = \alpha_0 \cdot \eta^{k/K}$, where α_0 is the initial learning rate, α_k is the learning rate for the current iteration, η is a hyper-parameter controlling the decay of learning rate, k is the current iteration step and K is the pre-defined total iteration step. For each iteration, three performance metrics are measured corresponding to base control command u^k, positive and negative perturbed control command $u^k \pm \delta u^k$, respectively.

We apply ASPGD with Hadamard basis to iteratively optimize soil imaging with Strehl ratio as the performance metric. We first divide the whole set of 812 Hadamard basis modes into different subsets, as shown in Fig. 4. Initialized at zero, ASPGD starts to optimize the first subset of Hadamard basis and we observe a rapid increase of Strehl ratio. This indicates that the first subset of 1-60 Hadamard basis modes has a large contribution to the soil phase representation and they are rapidly being corrected by ASPGD. Due to the orthogonal property of Hadamard basis set, we can freeze the Hadamard coefficients for the first subset of Hadamard modes and continue to optimize the second subset of Hadamard modes. The Strehl ratio continues to climb up, indicating that the 61-180 Hadamard basis modes are continuously being corrected by ASPGD. After a plateau is reached, we manually freeze this subset of Hadamard coefficients and move on to the third subset. The Strehl ratio continues to increase but slowly, which is consistent with the lower contribution of 181-300 Hadamard basis modes to soil phase representation. We continue the optimization with the remaining subsets of Hadamard basis,

and again, the Strehl ratio only has a marginal improvement even with nearly 1000 iteration steps.

The optimization curve with Hadamard basis in Fig. 4 resembles the PSF correction performance curve with truncated subset of Hadamard basis in Fig. 3(c), indicating that the optimization can find the coefficients for the Hadamard modes that closely fit the soil phase. Large Hadamard coefficients are primarily in the region of low spatial frequency, and most Hadamard coefficients in the region of high spatial frequency are small thus can be ignored with negligible loss of quality. Thanks to this feature, we could choose to just optimize certain subset of Hadamard basis, e.g., the first 300 Hadamard basis modes, which gives a good balance between correction performance and the optimization time. We can come back to re-optimize 61-180 Hadamard basis modes if needed without interfering with other Hadamard basis modes, which is shown at the last region of the optimization curve. This capability and flexibility cannot be achieved by using pixel basis.

To verify the faster convergence rate provided by Hadamard basis, we also conducted the ASPGD optimization in pixel basis with binning factor of 26, as shown Fig. 4. It shows that ASPGD with Hadamard basis has a clear advantage in the beginning stage of optimization and continues to overperform the ASPGD optimization with pixel basis. Quantitatively, optimization with Hadamard basis has an 1805 / 278 = 6.5 times higher convergence rate than that with pixel basis, which is calculated as the ratio of the iteration step needed with pixel basis to that with Hadamard basis to reach Strehl ratio of 24.3%. If we fix the iteration step of 1805, with Hadamard basis the Strehl ratio improves to 35.9%, instead of 24.3% obtained with pixel basis.

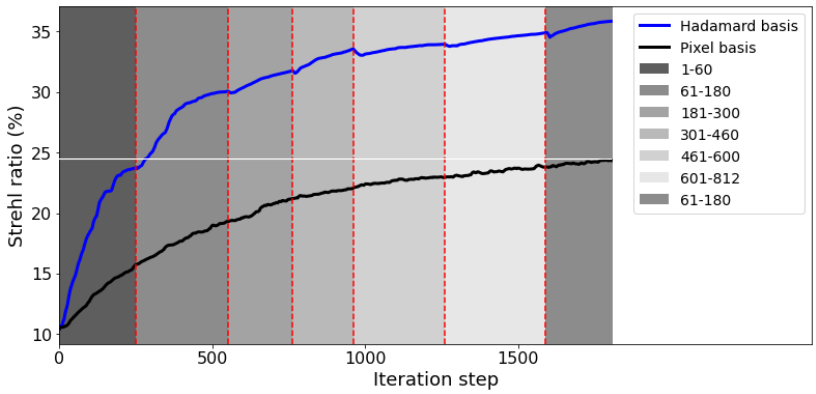

Fig. 4. ASPGD optimization with Hadamard basis converges 6.5x faster in simulation.

3.2 Experimental setup

The experimental setup of wavefront shaping for soil imaging is shown in Fig. 5. Light from a 632.8 nm He-Ne laser is collimated and expanded (not shown) before impinging on the SLM (Meadowlark, HSP1920-500-1200-HSP8). A half-wave-plate is used to rotate the polarization direction of the laser to make sure it matches the polarization direction of the SLM. Reflected light from SLM is modulated and the modulated wavefront is relayed by a 1:1 relay system to the entrance pupil plane of the objective (Mitutoyo, 20x, NA=0.42). The SLM is conjugate to the entrance pupil of the objective. The beam pupil on the SLM is a circle of diameter 848 pixels. The light is aberrated and scattered by the sample before reaching the focal plane. To prepare the sample, the synthetic smectite (Syn-1 Clay Minerals Society) was separated into the < 2 μm size fraction through centrifugation in deionized water using Stokes law. The < 2 μm size fraction was then flocculated using 2M NaCl and transferred into dialysis tubing to remove excess salts. The sample was then freeze dried overnight and then rehydrated with 0.5%

agarose and heated to 65°C. The agarose was used to maintain hydration of the Syn-1 during analysis and prevent the movement of the mineral particles. The Syn-1 agarose mixtures (1 g/mL) were then spread onto a microscope slide with a cover slip, pressed into thin films and sealed. A second objective Obj2 (Mitutoyo, 20x, NA=0.42) images the target focus and a CMOS camera (Hamamatsu, C13440-20CU) monitors the intensity distribution of the transmitted light in the target focus and provides feedback for our ASPGD algorithm to control the SLM.

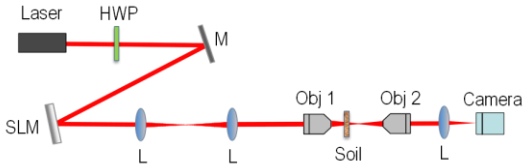

Fig. 5. Schematic of the experimental setup. L: lens, M: mirror, HWP: half-wave-plate.

3.3 Experimental results

To demonstrate the performance of our method in the real-world applications, we have implemented ASPGD with Hadamard basis in our experimental system and used it to focus through the soil mineral sample. The sample we are using is ~ 200 μm, located 5 mm from the target focus. The target focus is aberrated and scattered by the sample and the transmitted intensity distribution on the target plane is detected by the camera, as shown in Fig. 6(a).

We optimize the first 300 Hadamard modes, which are divided into 5 subsets with each subset containing 60 modes. Initialized at zero, we optimize the first subset, using the maximum intensity of the captured camera image as the performance metric. For each iteration, a perturbation step size for control basis mode is selected so that it matches the quantization on the SLM. To reduce the measurement noise, for each SLM phase pattern, we capture 4 frames and calculate the maximum intensity for each frame. We then remove the frames with the highest and lowest maximum intensity and use the averaged maximum intensity from the other two frames as the final maximum intensity. Starting at the initial point with maximum intensity of 752 with zero SLM pattern, a rapid increase of the performance metric is observed once the optimization starts, as shown in Fig. 6(g), where the ratio of improvement of the maximum intensity to its initial point is plotted. After a plateau is reached for the current subset of Hadamard basis, we manually freeze the current subset of Hadamard coefficients and continue the optimization with the next subset of Hadamard basis. The performance metric continues to increase and gradually reaches the overall plateau. At the end of optimization, an SLM phase pattern represented by 300 Hadamard basis modes is acquired as shown in Fig. 6(d), which results in a bright and tight focus of the final transmitted intensity distribution after the sample as shown in Fig. 6(b).

This is one example of the experimental results to demonstrate the optimization process. The performance of our proposed method is further verified in multiple repeated experiments with four out of five showing obvious advantages of using Hadamard basis (see supplementary materials).

To compare the above optimization performance with that using pixel basis, we also used pixel basis with binning factor of 26 as the control basis and conducted the ASPGD with this pixel basis to correct the same sample. In total, there are 849 binned pixels across the pupil being optimized. The corresponding optimization evolution curve is plotted in Fig. 6(g). We have swept a range of parameter choices and find $\alpha_0 = 0.06$ and $|\delta u^k| = 0.05$ give the best optimization performance with pixel basis. We use these two values during the optimization process. Starting at the maximum intensity of 1023, the optimization with pixel basis has a slow start in the beginning stage of optimization and continues to underperform the optimization

with Hadamard basis. The difference between the initial starting intensity of the optimization with Hadamard basis and that with pixel basis may be caused by the laser intensity fluctuation, SLM phase modulation variation, sample drift over time and the camera noise. The final SLM phase pattern expressed by the binned pixel found at the end of optimization and the resultant transmitted intensity distribution are shown in Fig. 6(e) and Fig. 6(c), respectively. Figure 6(c) shows a focus is formed but it is much dimmer than the focus in Fig. 6 (b), indicating the inferior optimization result comparing to that with Hadamard basis. Comparing Fig. 6(d) with Fig. 6(e), the SLM phase representation with Hadamard basis are dominant with lower spatial frequency structure and supplemented with higher spatial frequency information, which is consistent with the general spatial frequency characterization of the wavefront structure to correct the aberration and scattering from soil mineral sample; Whereas, the frequency distribution characterization doesn't appear on the SLM phase representation with pixel basis. To compare the convergence rate between the Hadamard basis and pixel basis, we chose the point where the optimization with pixel basis gives the best performance for the fairest comparison. Quantitatively, the optimization with Hadamard basis has a 523 / 71 = 7.4 times higher convergence rate than that with pixel basis, which is calculated as the ratio of the iteration step taken with pixel basis to reach its best performance to that with Hadamard basis to reach the same performance metric; If we fix the iteration step of 523, with Hadamard basis the performance metric improves by a factor of 3.5, whereas with pixel basis it only improves by a factor of 1.8.

The potential reasons for the slight difference between the convergence rate improvement factors in simulation and experiment are: first, the simulated soil wavefront is different from the soil wavefront in the real experiment. The simulated soil wavefront may not fully represent the soil wavefront in the real experiment. As we have observed in various experiments, different soil wavefront structures have slightly different optimization convergence rates; second, the achievable maximum quality enhancement is limited by the signal to noise ratio (SNR) for the experiments in a noisy environment [5]. Optimization with the Hadamard basis is less sensitive to noise errors, as previously reported in others' work [19,27,28]. Thus, the optimization with the Hadamard basis has a better performance and the optimization with pixel basis often saturates at a lower performance enhancement in the real experiment when the noise is not negligible.

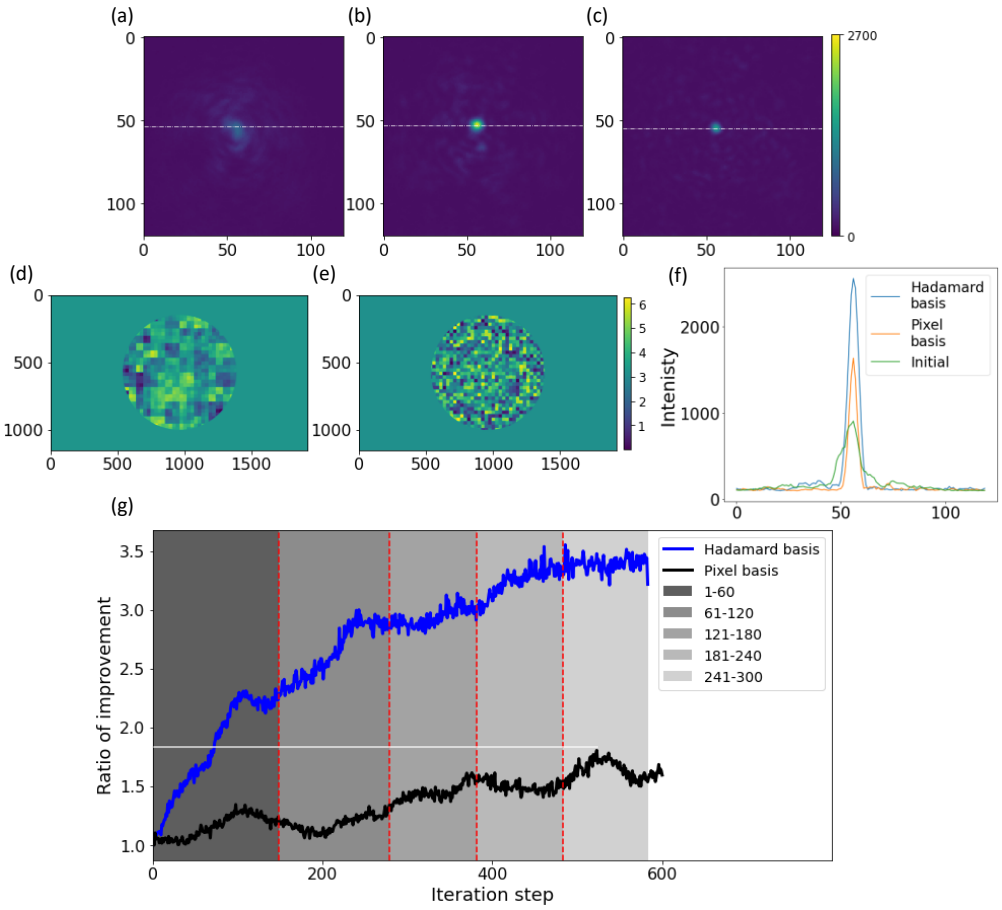

Fig. 6. Experimental results. (a). The transmitted intensity distribution of the target focus caused by the sample with SLM phase pattern equal to zero. (b). Final transmitted intensity distribution after the optimization with Hadamard basis. (c). Final transmitted intensity distribution after the optimization with pixel basis. (d). Final SLM phase pattern found by the optimization with Hadamard basis. (e). Final SLM phase pattern found by the optimization with pixel basis. (f). The intensity distribution plot along the rows where the maximum intensities locate. (g). The optimization evolution curve.

The advantage of the spatial frequency efficiency of the Hadamard basis in soil imaging that we are asserting comes from the fact that the soil samples at the scale we are interested in won't induce a fully randomly distorted wavefront. Soil phases have a structured power-law model. Therefore, the soil wavefront facilitates a sparse representation with the Hadamard basis, with lower-frequency Hadamard patterns having larger coefficients and the rest of the coefficients are negligibly small. This allows us to represent the soil wavefront with fewer basis modes, which leads to a faster optimization convergence rate.

We have used the first 300 Hadamard basis modes to represent the wavefront pattern. In the future work, we would like to explore what the optimal truncated set of Hamdard basis is for the best balance between performance and number of Hadamard basis modes used; we will also pursue generating the tailored basis specially for representing soil samples which is expected to dramatically reduce the basis modes needed for focusing light through soil samples, which is also expected to give a better correction performance and further increase the optimization convergence rate.

4. Conclusion

We have developed a wavefront shaping method based on ASPGD with the Hadamard basis for focusing light through soil samples. With Hadamard basis we can approximate the wavefront phase with fewer coefficients. This reduces the dimensionality of the soil phase representation and consequently reduces the optimization dimensionality of wavefront shaping in soil imaging with fewer control variables. Simulation results show that our method has a 6.5 times higher convergence rate and better optimization performance compared to that with pixel basis. Experimentally we have demonstrated ASPGD with Hadamard basis to focus light through soil mineral samples. The experimental results showed the ASPGD with Hadamard basis has a 7.4 times higher convergence rate and better overall correction performance than that with pixel basis. The proposed method is a general optimization approach which can benefit other high-dimensional optimization problems in adaptive optics and wavefront shaping.

Funding. U.S. Department of Energy Office of Biological and Environmental Research (SCW1652).

Acknowledgments. This work was performed under the auspices of the U.S. Department of Energy by Lawrence Livermore National Laboratory under Contract DE-AC52-07NA27344. Document #: LLNL-JRNL-826634

Disclosures. The authors declare no conflicts of interest.

Data availability. Data underlying the results presented in this paper are not publicly available at this time but may be obtained from the authors upon reasonable request.

See Supplement 1 for supporting content.

References

1. M. G. A. van der Heijden, R. D. Bardgett, and N. M. van Straalen, "The unseen majority: soil microbes as drivers of plant diversity and productivity in terrestrial ecosystems," Ecol. Lett. **11**, 296–310 (2008).
2. G. B. De Deyn, J. H. C. Cornelissen, and R. D. Bardgett, "Plant functional traits and soil carbon sequestration in contrasting biomes," Ecol. Lett. **11**, 516–531 (2008).
3. S. Herrera Paredes and S. L. Lebeis, "Giving back to the community: microbial mechanisms of plant–soil interactions," Funct. Ecol. **30**, 1043–1052 (2016).
4. R. J. Rodriguez, J. Henson, E. Van Volkenburgh, M. Hoy, L. Wright, F. Beckwith, Y.-O. Kim, and R. S. Redman, "Stress tolerance in plants via habitat-adapted symbiosis," ISME J. **2**, 404–416 (2008).
5. J. Kubby, S. Gigan, and M. Cui, eds., Wavefront Shaping for Biomedical Imaging, 1st ed. (Cambridge University Press, 2019).
6. I. M. Vellekoop and A. P. Mosk, "Focusing coherent light through opaque strongly scattering media," Opt. Lett. **32**, 2309 (2007).
7. I. M. Vellekoop, E. G. van Putten, A. Lagendijk, and A. P. Mosk, "Demixing light paths inside disordered metamaterials," Opt. Express **16**, 67 (2008).
8. D. B. Conkey, A. N. Brown, A. M. Caravaca-Aguirre, and R. Piestun, "Genetic algorithm optimization for focusing through turbid media in noisy environments," Opt. Express **20**, 4840 (2012).
9. I. M. Vellekoop and A. P. Mosk, "Phase control algorithms for focusing light through turbid media," Opt. Commun. **281**, 3071–3080 (2008).
10. A. J. Wright, D. Burns, B. A. Patterson, S. P. Poland, G. J. Valentine, and J. M. Girkin, "Exploration of the optimisation algorithms used in the implementation of adaptive optics in confocal and multiphoton microscopy," Microsc. Res. Tech. **67**, 36–44 (2005).
11. M. A. Vorontsov and V. P. Sivokon, "Stochastic parallel-gradient-descent technique for high-resolution wave-front phase-distortion correction," J. Opt. Soc. Am. A **15**, 2745 (1998).
12. G. Yang, L. Liu, Z. Jiang, J. Guo, and T. Wang, "Incoherent beam combining based on the momentum SPGD algorithm," Opt. Laser Technol. **101**, 372–378 (2018).
13. Q. Hu, L. Zhen, Y. Mao, S. Zhu, X. Zhou, and G. Zhou, "Adaptive stochastic parallel gradient descent approach for efficient fiber coupling," Opt. Express **28**, 13141 (2020).
14. S. Ma, P. Yang, B. Lai, C. Su, W. Zhao, K. Yang, R. Jin, T. Cheng, and B. Xu, "Adaptive Gradient Estimation Stochastic Parallel Gradient Descent Algorithm for Laser Beam Cleanup," Photonics **8**, 165 (2021).
15. D. P. Kingma and J. Ba, "Adam: A Method for Stochastic Optimization," ArXiv14126980 Cs (2017).
16. S. L. Brunton and J. N. Kutz, Data-Driven Science and Engineering: Machine Learning, Dynamical Systems, and Control (Cambridge University Press, 2019).

17. W. K. Pratt, J. Kane, and H. C. Andrews, "Hadamard transform image coding," Proc. IEEE **57**, 58–68 (1969).
18. Z. Zhang, X. Wang, G. Zheng, and J. Zhong, "Hadamard single-pixel imaging versus Fourier single-pixel imaging," Opt. Express **25**, 19619 (2017).
19. S. M. Popoff, G. Lerosey, R. Carminati, M. Fink, A. C. Boccara, and S. Gigan, "Measuring the Transmission Matrix in Optics: An Approach to the Study and Control of Light Propagation in Disordered Media," Phys. Rev. Lett. **104**, 100601 (2010).
20. S. Popoff, G. Lerosey, M. Fink, A. C. Boccara, and S. Gigan, "Image transmission through an opaque material," Nat. Commun. **1**, 81 (2010).
21. E. Premillieu and R. Piestun, "Measuring the transmission matrix of a scattering medium using epi-fluorescence light," Opt. Commun. **462**, 125207 (2020).
22. A. Escobet-Montalbán, R. Spesyvtsev, M. Chen, W. A. Saber, M. Andrews, C. S. Herrington, M. Mazilu, and K. Dholakia, "Wide-field multiphoton imaging through scattering media without correction," Sci. Adv. **4**, eaau1338 (2018).
23. P. T. Galwaduge, S. H. Kim, L. E. Grosberg, and E. M. C. Hillman, "Simple wavefront correction framework for two-photon microscopy of in-vivo brain," Biomed. Opt. Express **6**, 2997 (2015).
24. von F. Zernike, "Beugungstheorie des schneidenver-fahrens und seiner verbesserten form, der phasenkontrastmethode," Physica **1**, 689–704 (1934).
25. E. W. Cheney and D. Kincaid, Linear Algebra: Theory and Applications, 1. ed (Jones and Bartlett Publishers, 2009).
26. D. Wang, L. A. Poyneer, P. K. Weber, D. C. Chen, S. Ly, T. A. Laurence, J. Lee, S. M. Ammons, E. E. Nuccio, and J. Pett-Ridge, "Adaptive optics multiphoton microscope for imaging microbial processes in highly scattering soil and roots," in Imaging and Applied Optics Congress (OSA, 2020), p. OF2B.4.
27. E. Herbert, M. Pernot, G. Montaldo, M. Fink, and M. Tanter, "Energy-based adaptive focusing of waves: application to noninvasive aberration correction of ultrasonic wavefields," IEEE Trans. Ultrason. Ferroelectr. Freq. Control **56**, 2388–2399 (2009).
28. B. Mastiani and I. M. Vellekoop, "Noise-tolerant wavefront shaping in a Hadamard basis," Opt. Express **29**, 17534 (2021).

Wavefront shaping with Hadamard basis for scattering soil imaging: supplemental document

During the adaptive stochastic parallel gradient descent (ASPGD) optimization, the learning rate α and the amplitude of random perturbations $|\delta u^k|$ are critical to the optimization performance. They must be carefully chosen in order to obtain the optimal optimization performance. A value that is too small leads to painfully slow convergence, while a value that is too large can hinder convergence or even cause divergence. The parameter setting for the experimental results in Fig. 6 is listed in Table S1.

Table S1. Parameter setting for the experimental results in Fig. 6

Modes	α	$\lvert\delta u^k\rvert$
Hadamard 0-60	5	2
Hadamard 61-120	3	2
Hadamard 121-180	3	2
Hadamard 181-240	2	2
Hadamard 241-300	2	1.6
Pixel basis	0.06	0.05

To verify the repeatability of our method, we repeated the experiments for multiple times on the similar soil mineral samples, whose optimization evolution curves are plotted in Fig. S1. It successfully demonstrates the repeatability of our method with majority of the experimental results showing the obvious advantages of using Hadamard basis. For the results from repeated experiment 1 shown in Fig. S1(a), optimization with pixel basis performs unexpectedly well and the optimization with Hadamard basis just shows a marginal advantage. One of the possible reasons is that the phase map of the soil mineral sample in repeated experiment 1 contains less low spatial frequencies thus optimizing Hadamard modes with low spatial frequencies doesn't provide a rapid progress of the improvement of the performance metric. It can also be due to the sub-optimal parameter setting for Hadamard basis.

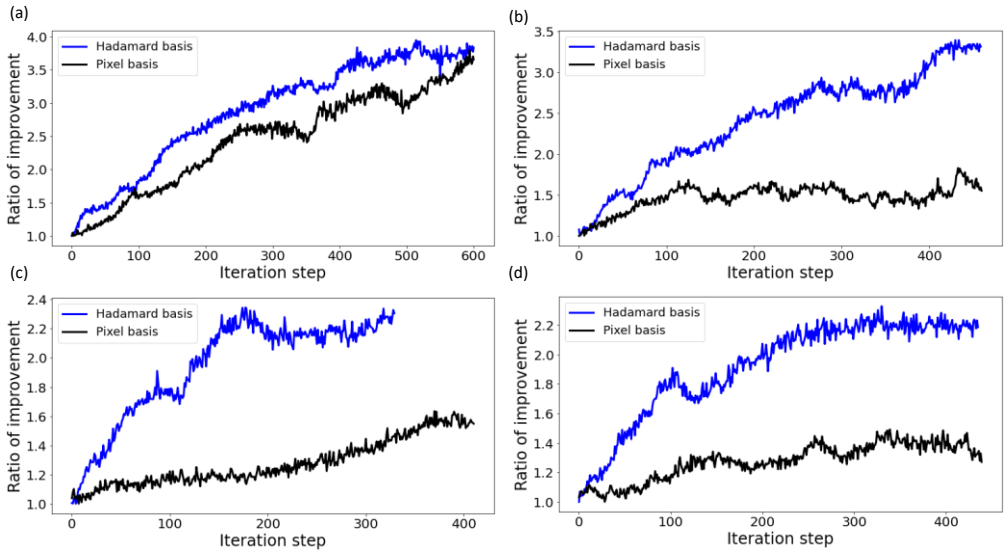

Fig. S1. The optimization evolution curves. (a). Repeated experiment 1. (b). Repeated experiment 2. (c). Repeated experiment 3. (d). Repeated experiment 4.

The found optimal parameter setting for the repeated experimental results in Fig. S1 is listed in Table S2. The optimal parameter setting varies for each experiment, which depend on the initial intensity distribution before optimization, the soil mineral sample under test and its optical aberration and scattering characteristics.

Table S2. Parameter setting for the repeated experimental results in Fig. S1

	Repeated Exp 1		Repeated Exp 2		Repeated Exp 3		Repeated Exp 4	
Modes	α	$\lvert\delta u^k\rvert$	α	$\lvert\delta u^k\rvert$	α	$\lvert\delta u^k\rvert$	α	$\lvert\delta u^k\rvert$
Hadamard 0-60	6	3	8	3	7	3	5	3
Hadamard 61-120	4	3	4	4	3	3	2	3
Hadamard 121-180	2.8	2.4						
Hadamard 181-240	2	2	1.6	4.5	0.8	3	1	3
Hadamard 241-300	1.6	1.6						
Pixel basis	0.06	0.05	0.07	0.05	0.04	0.05	0.05	0.05